

## Original article

# Molecular modeling on Gulong shale oil and wettability of reservoir matrix

FengLu Cui<sup>1</sup>, Xu Jin<sup>2</sup><sup>\*</sup>, He Liu<sup>2</sup>, HengAn Wu<sup>1</sup><sup>\*</sup>, FengChao Wang<sup>1</sup>

<sup>1</sup>CAS Key Laboratory of Mechanical Behavior and Design of Materials, Department of Modern Mechanics, University of Science and Technology of China, Hefei 230027, P. R. China

<sup>2</sup>PetroChina Research Institute of Petroleum Exploration & Development, Beijing 100083, P. R. China

### Keywords:

Shale oil  
molecular modeling  
oil-matrix interactions  
wetting  
molecular dynamics simulations

### Cited as:

Cui, F., Jin, X., Liu, H., Wu, H., Wang, F.  
Molecular modeling on Gulong shale oil  
and wettability of reservoir matrix.  
Capillarity, 2022, 5(4): 65-74.  
<https://doi.org/10.46690/capi.2022.04.01>

### Abstract:

Understanding molecular interactions between oil and reservoir matrix is crucial to develop a productive strategy for enhanced oil recovery. Molecular dynamics simulation has become an important method for analyzing microscopic mechanisms of some static properties and dynamic processes. However, molecular modeling of shale oil and reservoir matrix is still challenging, due to their complex features. Wettability, which is the measurement of oil-matrix interactions, requires in-depth understanding from the microscopic perspective. In this study, the density, interfacial tension and viscosity of eleven common components in shale oil are calculated using molecular dynamics simulations. Then a molecular model of Gulong shale oil is built, based on the reported experimental results and simulations. Compared with the variation in hydrocarbon content, the change in polar component content leads to more significant variations in the physical properties of shale oil. This molecular model is also employed to investigate the wettability of shale-oil nanodroplets on minerals and organic matter, with or without the surrounding aqueous phase. This work suggests fresh ideas for studying the oil-matrix interactions on the nanoscale and provides theoretical guidance for shale oil exploitation.

## 1. Introduction

With the increasing global energy demand, unconventional oil and gas have become an important part of the future energy structure (Zou et al., 2019). In August 2021, the discovery of Gulong shale oil was announced, and it attracted widespread attention due to its huge reserves (1.268 billion tonnes worth of geological reserves). The storage space of shale oil is highly heterogeneous, and the presence of hierarchical micro-nano pores has an important influence on the storage and transport of shale oil (Huai et al., 2020; Jin et al., 2021). Many classical theory and concepts, such as capillary condensation theory, multiphase seepage theory, contact line dynamics and contact angle are used to describe the mechanism of solid-liquid-gas interactions and enhanced oil recovery, which has been proposed as one of the six key scientific problems in the

production of Gulong shale oil (Sun et al., 2021). Meanwhile, the flow mechanisms of the fluid in pore which have been widely studied (Cai et al., 2014 and 2021; Liu et al., 2020;) play an important role in exploiting shale oil. Due to the small pore throat structure of shale oil reservoirs and the complex fluid phase state, the experimental investigations on shale oil have focused on the microscopic scale. To this end, Jin et al. (2021) analyzed the distribution of movable shale oil using the charge effect of electron beams, which is an intuitive manifestation of the difference in electrical conductivity of the specimens. Generally, the pore size of Gulong shale reservoir ranges from 10 to 50 nm, which were measured by the mercury injection method. However, field emission scanning electron microscopy observed the existence of shale oil in a pore with size of 9 nm, which breaks the knowledge that the lower limit of oil-bearing pore size is 20 nm (He et al., 2022). At the

same time, important progresses have been made in multi-scale digital core technologies such as mineral composition analysis and digital rock fracture propagation simulation (Jin et al., 2021). Because of the tight storage space of Gulong shale oil, the interface effect is expected to play a dominant role and the microscopic interactions between oil and reservoir matrix become quite important. In recent years, molecular dynamics (MD) simulation has proved itself a powerful research method in providing the atomic details of dynamic behaviors. Besides, it can calculate many physical properties and interfacial processes from a microscopic perspective, such as viscosity and interfacial tension of shale oil, adsorption and desorption behavior of oil film on the surface of rock. These results can be compared directly or indirectly with the experiments, which further provides a cross-scale and comprehensive understanding for the exploitation of shale oil.

The surface wettability is a significant manifestation of the strength of microscopic oil-rock interactions (Haagh et al., 2017). The wettability of shale oil on difference kinds of reservoir matrix determines the distribution of the shale oil in the micro-nano pores (Gong et al., 2016). The contact angle has been widely adopted to quantitatively describe the surface wettability. It has been reported that the measured contact angle shows a clear dependence on the oil component ratio (Zhong et al., 2013; Chang et al., 2018). Moreover, different drive methods may alter the wettability of reservoir matrix (Gong et al., 2016). For example, after the water or polymer drive, the wettability can be changed to the oil-wet state from the initial water-wet condition, which may block water channeling and thereby improve the sweep efficiency. On the other hand, the surface wettability also affects the flow characteristics of shale oil in nanopores, which are of great significance in the exploitation process (Golparvar et al., 2018; Zhang et al., 2019; Shaat et al., 2020; Sui et al., 2020; Hong et al., 2022).

In fact, the components of shale oil are quite complex, and an appropriate molecular model of shale oil is the first priority to obtain accurate understanding on the underlying physics based on MD simulations. Many previous MD studies used only individual hydrocarbon component to investigate the interactions between oil and reservoir matrix, rather than the mixed oil model (Falk et al., 2015; Wang et al., 2016; Zhao et al., 2019; Sui et al., 2020). However, the density, interfacial tension and viscosity of individual hydrocarbon can not reproduce the properties of real shale oil exactly. These properties are fundamental to recognize the dynamic process of shale oil exploitation. The viscosity is important for the characterization of heat, mass, and momentum transfer (Manjunatha et al., 2021). The interfacial tension is of particular relevance in wetting phenomena and mass transfer across phase boundaries. Accurate information on the viscosity and interfacial tension are also helpful to establish a reliable connection between MD simulations and experiments.

Low density (less than  $0.84 \text{ g/cm}^3$ ) and low viscosity (less than  $0.8 \text{ mPa}\cdot\text{s}$ ) are important characteristics of Gulong shale oil that distinguish it from other continental shale oils (Sun et al., 2021). The present work puts forward some suggestions on building the molecular model of Gulong shale oil, according

to the characteristics of SARA (saturate, aromatic, resin and asphaltene) components in shale oil (Cao et al., 2016; Wang et al., 2018). Density, interfacial tension and viscosity are calculated for not only each component separately, but also their mixture. Properties of shale oil with different component ratios are investigated to study the influence of individual component. At last, the wettability of nanodroplets of the modeled shale oil on various kinds of reservoir matrix are discussed, and the effect of aqueous phase on contact angle was analyzed. This work provides theoretical guidance for the extraction of shale oil.

## 2. Methodology and simulation

### 2.1 Model

The complexity of shale oil components must be considered in the modeling and simulations. Shale oil consists of hydrocarbons and non-hydrocarbons. Hydrocarbons are the main component of shale oil, including chain alkanes, naphthenes, benzene, etc. Non-hydrocarbons mainly include sulfur compounds, oxygenates and nitrogen compounds. Sulfur can appear in the form of hydrogen sulfide, mercaptan, sulfide, etc. The nitrogen-containing compounds identified in shale oil are mostly pyridine and quinoline. The oxygen-containing compounds can be divided into acidic oxygen-containing compounds and neutral oxygen-containing compounds. The former includes naphthenic acid, fatty acid, etc., while aldehydes and ketones belong to the latter. The first research objective of this work is to build a molecular model for shale oil according to the least experimental results of Gulong shale oil in Daqing Oilfield (Sun et al., 2021). Specifically, the asphaltenes can be neglected in the molecular modeling, because the mass proportion of asphaltene in Gulong shale oil is too small (generally  $< 0.4\%$ ). As a contrast, saturated hydrocarbons account for more than 80% of the total mass (Sun et al., 2021). The gas chromatographic analysis results show that the carbon chain of Gulong shale oil is short, and a length of 12 carbon atoms takes up a considerable portion. Thus dodecane is chosen as one of the representatives to model hydrocarbons in this work. Besides, ten other components are selected to build the molecular model of shale oil, as shown in Fig. 1(a)-1(k). All these eleven components can be classified into saturated hydrocarbons, aromatic hydrocarbons and resin. Hexane, dodecane, 3-methylpentane and methyl cyclohexane belong to saturated hydrocarbons, which will be abbreviated respectively as S1, S2, S3 and S4 in the subsequent context, as shown in Fig. 1(a)-1(d). As for aromatic hydrocarbons, A1 and A2 are used to denote benzene and toluene, which are shown in Fig. 1(e)-1(f). In a similar way, Heptanal, phenol, heptanoic acid, quinoline, and hexanethiol which are represented by R1, R2, R3, R4 and R5 are constituent parts of resin, as shown in Fig. 1(g)-1(k). These components have been widely used to study shale oil in MD simulations (Mikami et al., 2013; Sedghi et al., 2016; Tian et al., 2018; Xiong et al., 2019; Abdel-Azeim et al., 2021; Zhang and Guo., 2021).

X-ray diffraction and nuclear magnetic resonance characterizations have reported that shale oil reservoirs contain both organic matter, i.e., kerogen (Xu et al., 2021) and a variety of

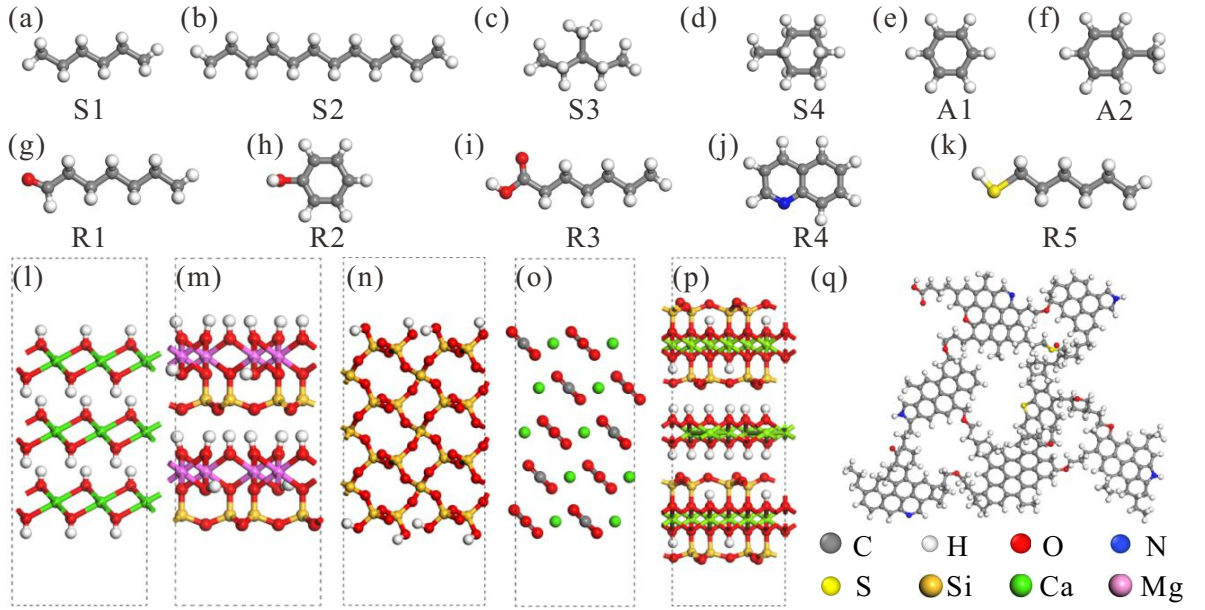


**Fig. 1.** Schematic diagram of shale oil components (a-k) and reservoir matrixes (l-q). (a) hexane (S1), (b) dodecane (S2), (c) 3-methylpentane (S3), (d) methyl cyclohexane (S4), (e) benzene (A1), (f) toluene (A2), (g) heptanal (R1), (h) phenol (R2), (i) heptanoic acid (R3), (j) quinoline (R4), (k) hexanethiol (R5), (l) portlandite, (m) kaolinite, (n) quartz, (o) calcite, (p) chlorite, (q) kerogen.

inorganic minerals, such as quartz, calcite and clays (Wu et al., 2015; Wang et al., 2018). In this study, quartz, portlandite, calcite, chlorite and kaolinite are selected to analyze the interactions between shale oil and inorganic minerals. The schematics of these molecular structure are shown in Fig. 1(l)-1(q).

## 2.2 Simulation method

In presented MD simulations, the atomic interactions were modeled by 12-6 Lennard-Jones potential coupled with a polar term to consider both the van der Waals and Coulombic forces (Fennell et al., 2006; Chen et al., 2019). The potential energy was calculated using the following formula:

$$E = 4\epsilon \left[ \left( \frac{\sigma}{r} \right)^{12} - \left( \frac{\sigma}{r} \right)^6 \right] + \frac{Cq_i q_j}{\epsilon_0 r} \quad r < r_c \quad (1)$$

where  $\epsilon$  is the energy parameter, kcal/mol;  $\sigma$  is the length parameter, Å;  $q_i$  and  $q_j$  are the charges on atom  $i$  and  $j$ , e;  $C$  is an energy-conversion constant, and  $\epsilon_0$  is the dielectric constant,  $C^2/(N \cdot m^2)$ ;  $r$  is the distance between two atoms, Å;  $r_c$  is the cutoff distance for the van der Waals and short-range electrostatic forces, which is set to be 12 Å. The long-range Coulombic interactions are calculated using particle-particle-mesh solver (Kelkar et al., 2007), which evaluates Fourier series directly with a desired relative error in forces of  $1 \times 10^{-4}$ . The ClayFF force field was used to describe the minerals (Cygan et al., 2004), while the oil molecules were simulated by OPLS-AA force field (Siu et al., 2012). All the MD simulations were implemented by LAMMPS (Plimpton, 1995).

To calculate the shear viscosity of shale oil, the Green-Kubo method based on equilibrium MD simulations was employed (Sun and Bai, 2018). The shear viscosity  $\eta$  (Pa·s) is calculated from an integral over time of the pressure tensor autocorrelation function:

$$\eta = \frac{V}{k_B T} \int_0^\infty \langle \sigma_{xy}(t) \sigma_{xy}(t) \rangle dt \quad (2)$$

where  $V$  is system volume,  $m^3$ ;  $k_B$  is Boltzmann constant;  $T$  is temperature, K;  $\sigma_{xy}$  is pressure tensor component, Pa;  $\langle \rangle$  denotes the time correlation function.

The interfacial tension  $\gamma_{LV}$  (N·m) was calculated using the method proposed by Kirkwood and Buff (Kirkwood et al., 1949), that is, integrating the stress difference along the vertical direction ( $z$ -axis) of a liquid film:

$$\gamma_{LV} = \int_{-\infty}^{+\infty} [P_N(z) - P_T(z)] dz \quad (3)$$

where  $P_N(z)$  and  $P_T(z)$  are the normal stress and tangential stress of the atom at coordinate  $z$ , Pa, respectively, as shown in Fig. 2(a).

## 3. Results and discussion

### 3.1 Physical properties of individual oil component

The physical properties of eleven components were calculated under two different conditions. One is normal temperature (300 K) and pressure (1 atmosphere), which is referred to as NTP. The other one is formation temperature (400 K) and pressure (33 atmosphere), abbreviated as FTP (He et al.,

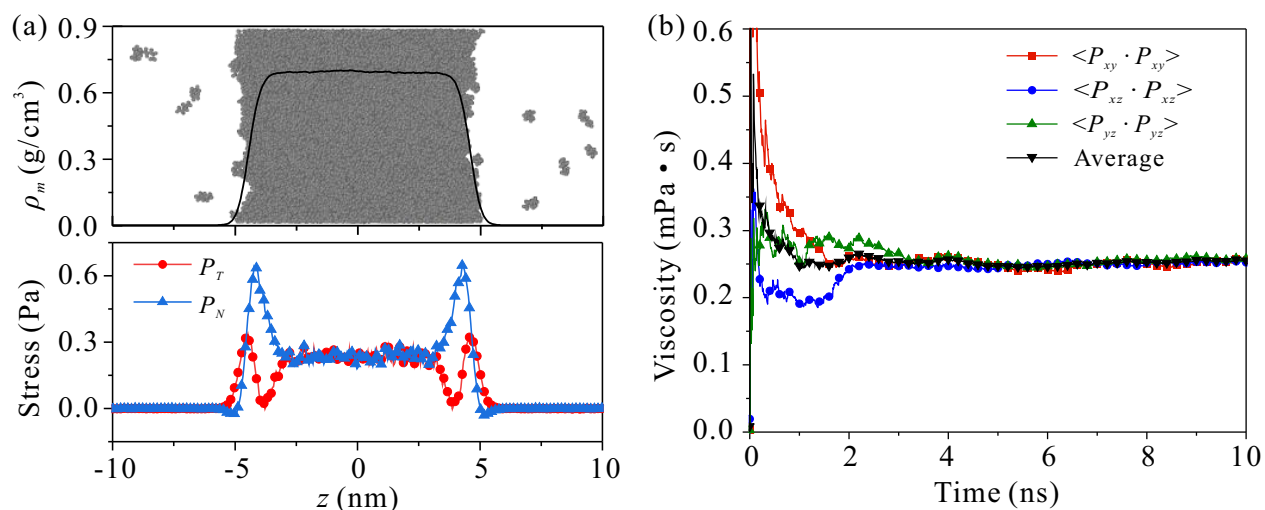


**Fig. 2.** (a) Density distribution ( $\rho_m$ ), tangential stress ( $P_T$ ) and normal stress ( $P_N$ ) of an oil film along the  $z$  direction at 400 K, 33 MPa. The black line represents the mass density distribution. Blue and red lines represent the normal and tangential stress, respectively. (b) Variation of the calculated viscosity of shale oil with simulation time. The red, green and blue lines show the shear viscosity in the three directions, and the black line is the average.

2022). The density of each component were summarized in Table 1. The MD results of interfacial tension and viscosity are provided Tables 2 and 3, respectively. In addition, these MD results are compared with the experimental data (Ma et al., 2013), and the relative deviation (RD) is given.

Table 1 shows that the density of all components at FTP are smaller than the density at NTP. In conventional knowledge, the increase in pressure would lead to an increment in the density of liquid, while the increasing temperature decreases the liquid density. The density reduction indicates that the temperature is dominant over pressure in influencing the density of shale oil. In addition, the increase in the carbon chain will result in larger density. The densities of S1 ( $0.63 \text{ g/cm}^3$ ) and S3 ( $0.64 \text{ g/cm}^3$ ) under NTP shows that the branched chains have an insignificant effect on the density. We can also speculate from Table 1 that, for the same length of carbon chain, the density of non-hydrocarbon compounds is generally larger than that of hydrocarbon compounds due to stronger van der Waals interactions between the molecules of non-hydrocarbon.

To calculate the interfacial tension, an oil film with a vacuum layer in  $z$  direction was constructed. Then the tangential, normal stresses and the mass density distribution in the  $z$  direction were calculated, as shown in Fig. 2(a). When calculating the viscosity, the isothermal-isobaric ensemble was used to control the temperature and pressure for 0.2 ns. Then, equilibrium MD simulations were conducted under the isochoric-isothermal ensemble with a Nose-Hoover thermostat. The accuracy of the Green-Kubo method to calculate the viscosity depends on the average number of stress-tensor auto-correlations. Simulations show that a relatively stable value of viscosity can be obtained by averaging the autocorrelation for 2000 times, as shown in Fig. 2(b). Analogous to the analysis on density, we found that the length of carbon chain has more noticeable influence on interfacial tension and viscosity, while

the effect of branched chains is not significant. The interfacial tension of polar compounds is larger than that of hydrocarbon compounds. Besides, the viscosity of polar compound can reach ten times more than that of hydrocarbon compound, albeit with similar carbon chain length. The underlying physics can be explained by the difference in surface electrostatic potential. Polar functional groups will result in stronger attraction between molecules than the neutral functional groups.

### 3.2 Molecular model of shale oil with mixed components

Experiments have confirmed that the content of saturated hydrocarbon, aromatic hydrocarbon, resin and asphaltene in Gulong shale oil was 84.2%, 9.7%, 8.0%~18.6% and less than 0.4%, respectively (Sun et al., 2021). These results provide us key benchmarks to build the molecular model. According to the experiments, the mass ratio of saturated hydrocarbons (75%), aromatic hydrocarbons (10%) and resins (15%) was first considered in this work. Then the number ratio of each component can be determined. For saturated hydrocarbons, the four components were mixed in the same mass ratio, but different number of molecules. The same rule was implemented for aromatic hydrocarbons and resins. Based on this proposed strategy, the molecular model of Gulong shale oil was provided here, as shown in Fig. 3. This model consisting of 1,000 molecules was put in a cubic box with a side length of 6 nm, containing 214 hexane (S1), 108 dodecane (S2), 247 3-methylpentane (S3), 187 methyl cyclohexane (S4), 63 benzene (A1), 53 toluene (A2), 26 heptanal (R1), 31 phenol (R2), 23 heptanoic acid (R3), 23 quinoline (R4) and 25 hexanethiol (R5). The model can be scaled up according to specific requirements.

Then, the density, interfacial tension and viscosity of this modeled shale oil were calculated in MD simulations under

both NTP and FTP. At NTP, the density is  $0.74 \text{ g/cm}^3$ , the interfacial tension is  $15.33 \text{ mN/m}$  and the viscosity is  $0.44 \text{ mPa}\cdot\text{s}$ , while the density, interfacial tension and viscosity are  $0.72 \text{ g/cm}^3$ ,  $5.34 \text{ mN/m}$  and  $0.26 \text{ mPa}\cdot\text{s}$  at FTP, respectively. The MD results are in good agreement with the density (less than  $0.84 \text{ g/cm}^3$ ) and viscosity (less than  $0.80 \text{ mPa}\cdot\text{s}$ ) of Gulong Shale oil derived from the experiments (Sun et al., 2021). When the simulation condition changed from NTP to FTP, the density was reduced by only 2.7%, while the interfacial tension was reduced by 65.2% and the viscosity was reduced by 40.9%. Combined with the results shown in Tables 1-3, the interfacial tension and viscosity of shale oil are more sensitive to temperature than to pressure.

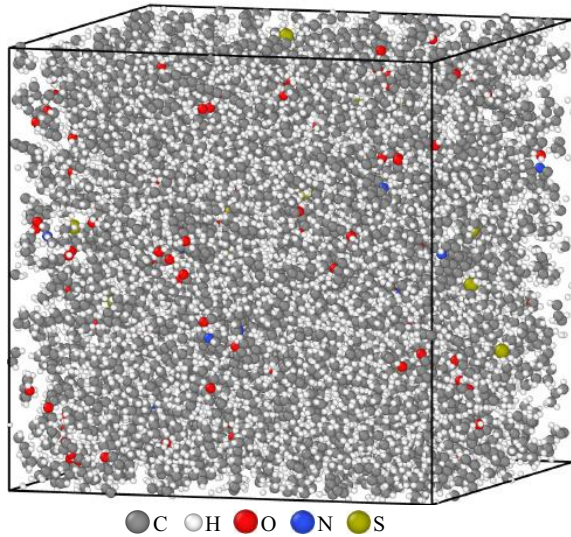


**Fig. 3.** Molecular model of shale oil with mixed components. Gray, white, red, blue and green represent carbon, hydrogen, oxygen, nitrogen and sulfur, respectively.

### 3.3 Influence of individual component

MD results given in Tables 1-3 have shown that the properties varies with different individual components. It is anticipated that the overall properties of shale oil depends on the content of each component. For this reason, here the influence of certain substance was analyzed. Hexane (S1) has relatively lower density, interfacial tension and viscosity, which is about only 80% or less of the mixed model given in Fig. 3. If the hexane (S1) content increases, the density, interfacial tension and viscosity of shale oil decrease accordingly, as shown in Fig. 4(a). On the contrary, phenol (R2) exhibits relatively higher density, interfacial tension and viscosity, compared with other components. Consequently, with the increase of phenol (R2) content, the density, interfacial tension and viscosity of shale oil will increase obviously, as shown in Fig. 4(b). In order to present all data in the same plot, all quantities are normalized using  $\rho^* = \rho/\rho_0$ ,  $\gamma^* = \gamma/\gamma_0$ ,  $\eta^* = \eta/\eta_0$ , in which  $\rho_0 = 1.5 \text{ g/cm}^3$ ,  $\gamma_0 = 10 \text{ mN/m}$ ,  $\eta_0 = 0.4 \text{ mPa}\cdot\text{s}$ . The change in phenol (R2) content has a greater influence on the physical properties of shale oil, indicating that the content of polar substances is an important factor affecting the physical properties of shale oil. This analysis suggests that it is feasible to predict the overall properties of shale oil based on the properties and contents of individual component.

### 3.4 Microscopic wettability

The contact angle of oil droplets on solid surface is an important index to intuitively quantify the interaction strength between shale oil and reservoir matrix. Smaller contact angle manifests stronger oil-reservoir interactions. With the suggested molecular model for Gulong shale oil provided in Fig. 3, here we turn to investigate the contact angle of shale oil on kerogen and five inorganic minerals (quartz, kaolinite, calcite, chlorite and portlandite). To eliminate the line tension effect, shale oil nanodroplets were built up into cylindrical

**Table 1.** Density of eleven components at NTP and FTP.

Component	NTP (300 K, 1 atm)			FTP (400 K, 33 atm)		
	MD ( $\text{g/cm}^3$ )	Reference ( $\text{g/cm}^3$ )	RD (%)	MD ( $\text{g/cm}^3$ )	Reference ( $\text{g/cm}^3$ )	RD (%)
S1	0.63	0.65	-3.07	0.60	0.56	7.14
S2	0.81	0.74	9.46	0.73	0.67	8.96
S3	0.64	0.66	-3.03	0.52	0.58	-10.34
S4	0.81	0.76	6.58	0.74	0.68	8.82
A1	0.85	0.87	-2.30	0.70	0.77	-9.09
A2	0.83	0.86	-3.49	0.78	0.77	1.30
R1	0.80	0.82	-2.44	0.75	-	-
R2	1.06	1.07	-0.94	0.97	0.98	1.02
R3	0.91	0.92	-1.09	0.87	-	-
R4	1.13	1.10	2.73	1.07	-	-
R5	0.81	0.84	-3.57	0.76	-	-

**Table 2.** Interfacial tension of eleven components at NTP and FTP.

Component	NTP (300 K, 1 atm)			FTP (400 K, 33 atm)		
	MD (mN/m)	Reference (mN/m)	RD (%)	MD (mN/m)	Reference (mN/m)	RD (%)
S1	12.26	17.70	-30.72	3.98	-	-
S2	19.06	24.75	-22.99	10.08	-	-
S3	12.81	17.41	-26.44	3.68	-	-
S4	32.23	23.08	39.67	20.08	-	-
A1	20.29	-	-	8.01	-	-
A2	20.38	27.71	-26.45	9.12	-	-
R1	22.48	26.17	-14.10	12.75	-	-
R2	33.90	40.67	-16.65	22.98	30.51	-24.68
R3	26.38	27.60	-4.43	17.60	-	-
R4	60.49	42.40	42.68	39.71	-	-
R5	17.99	-	-	7.52	-	-

**Table 3.** Viscosity of eleven components at NTP and FTP.

Component	NTP (300 K, 1 atm)			FTP (400 K, 33 atm)		
	MD ( $\mu\text{Pa}\cdot\text{s}$ )	Reference ( $\mu\text{Pa}\cdot\text{s}$ )	RD (%)	MD ( $\mu\text{Pa}\cdot\text{s}$ )	Reference ( $\mu\text{Pa}\cdot\text{s}$ )	RD (%)
S1	212.77	294.21	-27.68	168.85	131.22	28.68
S2	697.45	1339.31	-47.92	388.00	419.12	-7.43
S3	275.61	280.25	1.66	187.68	159.47	17.69
S4	849.41	662.65	28.18	473.71	269.65	75.68
A1	489.13	584.53	-16.32	134.94	214.44	-37.07
A2	414.66	536.60	-22.72	267.07	239.85	11.35
R1	580.87	-	-	363.91	-	-
R2	3527.14	3169.35	11.30	817.71	788.42	3.77
R3	1999.80	3680.69	-45.67	649.59	-	-
R4	1294.03	3169.34	-59.17	657.86	633.91	3.79
R5	386.41	-	-	243.18	-	-

shapes with an initial radius of 4 nm (Fan et al., 2020). The simulations were conducted in the isochoric-isothermal ensemble with a temperature of 300 K. Periodic boundary conditions were applied in the  $x$  and  $y$  directions, while the reflective boundary condition is applied in the  $z$  direction. At the beginning, the shale oil droplet was located on top of the matrix with a certain distance. After the equilibrium simulation, the oil droplet gradually approached and then spread on the matrix surface because of the oil-matrix attraction. The contact angle can be calculated using the density profiles averaged over the cross section of the cylindrical oil droplet perpendicular to its axis. By fitting the oil droplet shape to a circle, the contact angle was obtained by calculating the

angle between the tangent of the circle and the horizontal line defining the matrix surface. If the oil droplets are spread completely into an oil film on the matrix surface, the contact angle is defined to be  $0^\circ$ , as shown in Fig. 5(a)-5(d). The contact angles of shale oil on quartz, and portlandite are  $16^\circ$  and  $36^\circ$ , respectively, as shown in Fig. 5(e)-5(f), indicating a weaker oil-mineral interactions in these two cases.

The contact angle of oil droplets on these matrixes are calculated with the surrounding aqueous phase. Oil-water-solid interactions are widely involved in reservoir storage and in the process of shale oil exploitation by water-driven methods (Myint et al., 2015). Therefore, it is necessary to investigate the influence of water. The simulations show that the contact angle

of the oil droplets in the aqueous phase changes significantly compared to the oil droplets without aqueous phase as shown in Fig. 6. In the surrounding aqueous phase, the matrix surface changes from oleophilic to hydrophilic, which makes shale oil easier to peel off the matrix surface. It also explains the reason why water driving can enhance oil recovery. For example, the contact angle of the oil droplets on the calcite surface changes from  $0^\circ$  to  $180^\circ$ , indicating that the wettability of the calcite surface is reversed. According to Young's equation, the contact angle reflects the equilibrium of interfacial tensions at

the three-phase junction (Young, 1805). The presence of water affects the oil-water and water-matrix interfacial tensions, hence changes the contact angle of the oil droplets. However, the amount of change in contact angle induced by water can not be predicted directly from MD simulations. For example, the contact angle of oil droplets on quartz varied from  $16^\circ$  to  $180^\circ$ , while it changed from  $36^\circ$  to  $110^\circ$  on portlandite surface. The effect of water on the interfacial tension still requires further investigation.

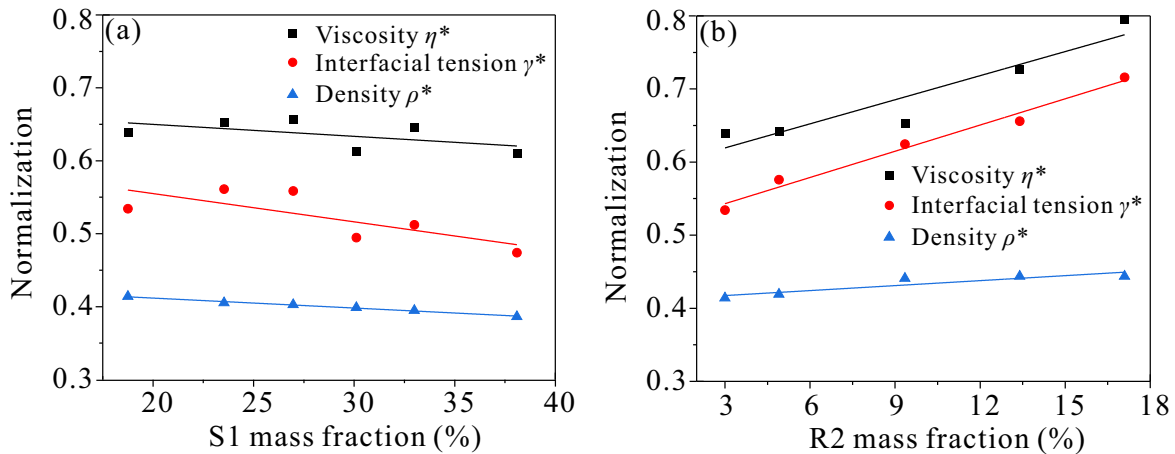


**Fig. 4.** (a) Variation of density, interfacial tension and viscosity of shale oil with increasing mass fraction of hexane (S1). (b) Variation of density, interfacial tension and viscosity of shale oil with increasing mass fraction of phenol (R2). For simplicity, the properties are all normalized using  $\rho^* = \rho/\rho_0$ ,  $\gamma^* = \gamma/\gamma_0$ ,  $\eta^* = \eta/\eta_0$ , in which  $\rho_0 = 1.5 \text{ g/cm}^3$ ,  $\gamma_0 = 10 \text{ mN/m}$ ,  $\eta_0 = 0.4 \text{ mPa}\cdot\text{s}$ .

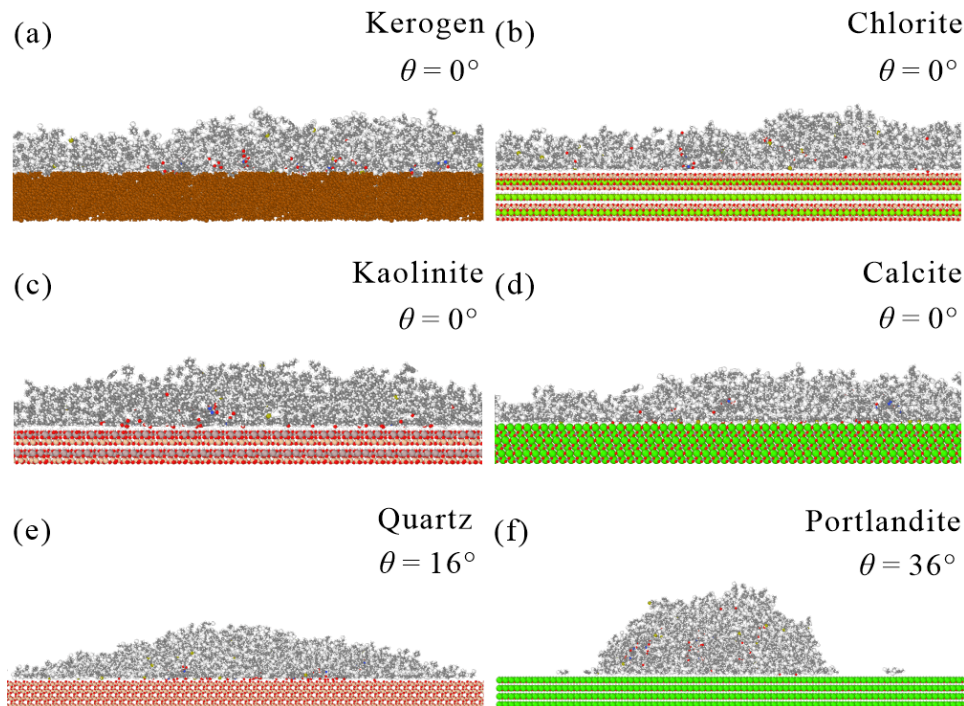


**Fig. 5.** Contact angle of shale oil nanodroplet. (a) kerogen,  $\theta = 0^\circ$ , (b) chlorite,  $\theta = 0^\circ$ , (c) kaolinite,  $\theta = 0^\circ$ , (d) calcite,  $\theta = 0^\circ$ , (e) quartz,  $\theta = 16^\circ$ , (f) portlandite,  $\theta = 36^\circ$ .

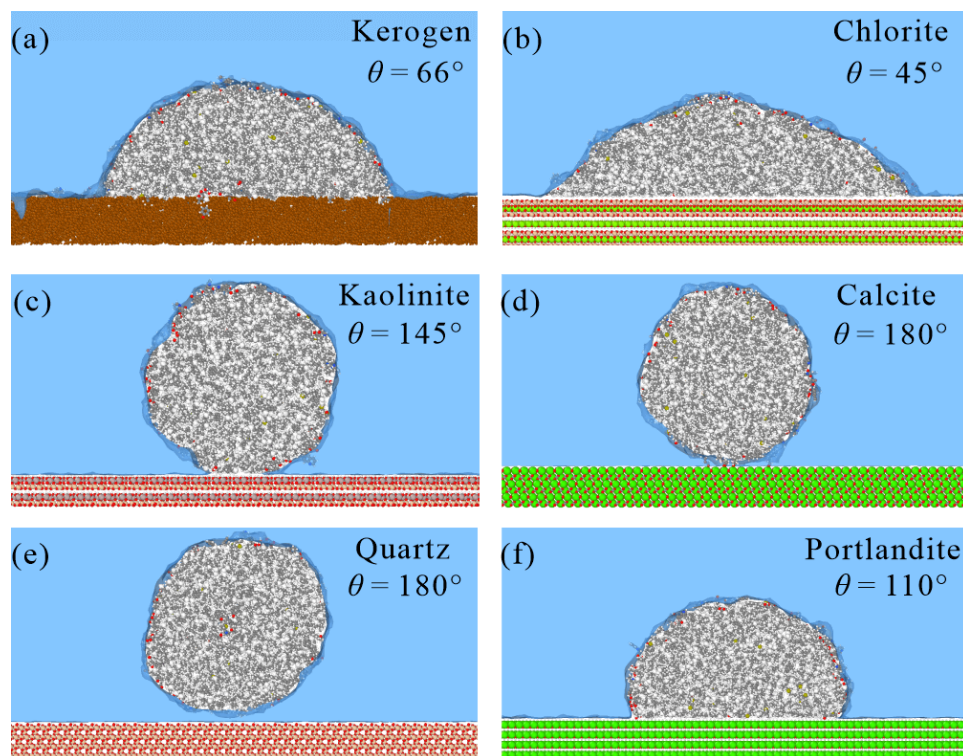


**Fig. 6.** Contact angle of shale oil nanodroplet in aqueous phase. (a) kerogen,  $\theta = 66^\circ$ , (b) chlorite,  $\theta = 45^\circ$ , (c) kaolinite,  $\theta = 145^\circ$ , (d) calcite,  $\theta = 180^\circ$ , (e) quartz,  $\theta = 180^\circ$ , (f) portlandite,  $\theta = 110^\circ$ .

#### 4. Conclusions

In this study, a molecular model of Gulong shale oil was proposed based on recent experimental results. The density, interfacial tension and viscosity was calculated and show good agreement with experiments. The influence of the properties of individual component was discussed. Compared with hydrocarbon compounds, polar compounds have a greater influence on the physical properties of shale oil. The wettability of shale oil reservoirs was investigated from a microscopic perspective. For kerogen, chlorite, kaolinite and calcite, oil droplets spread completely into an oil film on the matrix surface, which manifests strong interactions. However, in the aqueous phase, the contact angle of the oil droplets changes significantly, indicating that the matrix surface changes from oleophilic to hydrophilic, which may explain the reason why water driving can enhance oil recovery. This work provides methodological guidance for analyzing the interaction between shale oil and reservoir matrix using MD simulation.

#### Acknowledgement

This work was financially supported by the National Key Research and Development Program of China (No. 2019YFA0708700), the National Natural Science Foundation of China (No. 11922213) and the Youth Innovation Promotion Association CAS (No. 2020449). The numerical calculations were performed on the supercomputing system in Hefei Advanced Computing Center and the Supercomputing Center of University of Science and Technology of China.

#### Conflict of interest

The authors declare no competing interest.

**Open Access** This article is distributed under the terms and conditions of the Creative Commons Attribution (CC BY-NC-ND) license, which permits unrestricted use, distribution, and reproduction in any medium, provided the original work is properly cited.

#### References

- Abdel-Azeim, S., Sakthivel, S., Kandiel, T. A., et al. Specificity and synergy at the oil-brine interface: New insights from experiments and molecular dynamics simulations. *Energy & Fuels*, 2021, 35(18): 14647-14657.
- Cai, J., Jin, T., Kou, J., et al. Lucas–Washburn equation-based modeling of capillary-driven flow in porous systems. *Langmuir*, 2021, 37(5): 1623-1636.
- Cai, J., Perfect, E., Cheng, C., et al. Generalized modeling of spontaneous imbibition based on Hagen–Poiseuille flow in tortuous capillaries with variably shaped apertures. *Langmuir*, 2014, 30(18): 5142-5151.
- Cao, Z., Liu, G., Kong, Y., et al. Lacustrine tight oil accumulation characteristics: Permian Lucaogou Formation in Jimusaer Sag, Junggar Basin. *International Journal of Coal Geology*, 2016, 153: 37-51.
- Chang, X., Xue, Q., Li, X., et al. Inherent wettability of different rock surfaces at nanoscale: A theoretical study. *Applied Surface Science*, 2018, 434: 73-81.
- Chen, C., Jiang, X., Sui, Y. Prediction of transport properties of fuels in supercritical conditions by molecular dynamics simulation. *Energy Procedia*, 2019, 158: 1700-1705.

- Cygan, R. T., Liang, J., Kalinichev, A. G. Molecular models of hydroxide, oxyhydroxide, and clay phases and the development of a general force field. *Journal of Physical Chemistry B*, 2004, 108(4): 1255-1266.
- Falk, K., Coasne, B., Pellenq, R., et al. Subcontinuum mass transport of condensed hydrocarbons in nanoporous media. *Nature Communications*, 2015, 6(1): 6949.
- Fan, J., Coninck, J. D., Wu, H., et al. Microscopic origin of capillary force balance at contact line. *Physical Review Letters*, 2020, 124(12): 125502.
- Fennell, C. J., Gezelter, J. D. Is the Ewald summation still necessary? Pairwise alternatives to the accepted standard for long-range electrostatics. *Journal of Chemical Physics*, 2006, 124(23): 234104.
- Golparvar, A., Zhou, Y., Wu, K., et al. A comprehensive review of pore scale modeling methodologies for multiphase flow in porous media. *Advances in Geo-Energy Research*, 2018, 2(4): 418-440.
- Gong, H., Li, Y., Dong, M., et al. Effect of wettability alteration on enhanced heavy oil recovery by alkaline flooding. *Colloids and Surfaces A: Physicochemical and Engineering Aspects*, 2016, 488: 28-35.
- Haagh, M. E. J., Sîretanu, I., Duits, M. H. G., et al. Salinity-dependent contact angle alteration in oil/brine/silicate systems: the critical role of divalent cations. *Langmuir*, 2017, 33(14): 3349-3357.
- He, W., Meng, Q., Feng, Z., et al. In-situ accumulation theory and exploration & development practice of Gulong shale oil in Songliao Basin. *Acta Petrolei Sinica*, 2022, 43(1): 1-14. (in Chinese)
- Huai, J., Xie, Z., Li, Z., et al. Displacement behavior of methane in organic nanochannels in aqueous environment. *Capillarity*, 2020, 3(4): 56-61.
- Hong, X., Yu, H., Xu, H., et al. Competitive adsorption of asphaltene and n-heptane on quartz surfaces and its effect on crude oil transport through nanopores. *Journal of Molecular Liquids*, 2022, 359: 119312.
- Jin, X., Li, G., Meng, S., et al. Microscale comprehensive evaluation of continental shale oil recoverability. *Petroleum Exploration and Development*, 2021, 48(1): 256-268.
- Kelkar, M. S., Rafferty, J. L., Maginn, E. J., et al. Prediction of viscosities and vapor-liquid equilibria for five polyhydric alcohols by molecular simulation. *Fluid Phase Equilibria*, 2007, 260(2): 218-231.
- Kirkwood, J. G., Buff, F. P. The statistical mechanical theory of surface tension. *Journal of Chemical Physics*, 1949, 17(3): 338-343.
- Liu, H., Zhu, Z., Patrick, W., et al. Pore-scale numerical simulation of supercritical CO<sub>2</sub> migration in porous and fractured media saturated with water. *Advances in Geo-Energy Research*, 2020, 4(4): 419-434.
- Ma, P., Xia, S., Xia, Q. *Concise Manual of Chemical Property Data*. Beijing, China, Chemical Industry Press, 2013. (in Chinese)
- Manjunatha, L., Takamatsu, H., Cannon, J. J. Atomic-level breakdown of Green-Kubo relations provides new insight into the mechanisms of thermal conduction. *Scientific Reports*, 2021, 11: 5597.
- Mikami, Y., Liang, Y., Matsuoka, T., et al. Molecular dynamics simulations of asphaltenes at the oil-water interface: From nanoaggregation to thin-film formation. *Energy & Fuels*, 2013, 27(4): 1838-1845.
- Myint, P. C., Firoozabadi, A. Thin liquid films in improved oil recovery from low-salinity brine. *Current Opinion in Colloid & Interface Science*, 2015, 20(2): 105-114.
- Plimpton, S. Fast parallel algorithms for short-range molecular dynamics. *Journal of Computational Physics*, 1995, 117(1): 1-19.
- Sedghi, M., Piri, M., Goual, L. Atomistic molecular dynamics simulations of crude oil/brine displacement in calcite mesopores. *Langmuir*, 2016, 32(14): 3375-3384.
- Shaht, M., Javed, U., Faroughi, S. Wettability and confinement size effects on stability of water conveying nanotubes. *Scientific Reports*, 2020, 10: 17167.
- Siu, S. W. I., Pluhackova, K., Böckmann, R. A. Optimization of the OPLS-AA force field for long hydrocarbons. *Journal of Chemical Theory and Computation*, 2012, 8(4): 1459-1470.
- Sui, H., Zhang, F., Wang, Z., et al. Molecular simulations of oil adsorption and transport behavior in inorganic shale. *Journal of Molecular Liquids*, 2020, 305: 112745.
- Sun, C., Bai, B. Improved CO<sub>2</sub>/CH<sub>4</sub> separation performance in negatively charged nanoporous graphene membranes. *Journal of Physical Chemistry C*, 2018, 122(11): 6178-6185.
- Sun, L., Liu, H., He, W., et al. An analysis of major scientific problems and research paths of Gulong shale oil in Daqing Oilfield, NE China. *Petroleum Exploration and Development*, 2021, 48(3): 527-540.
- Tian, S., Erastova, V., Lu, S., et al. Understanding model crude oil component interactions on kaolinite silicate and aluminol surfaces: Toward improved understanding of shale oil recovery. *Energy & Fuels*, 2018, 32(2): 1155-1165.
- Wang, Q., Qin, Y., Jia, W., et al. Density and viscosity of tight oil from Yanchang Formation, Ordos Basin, China and the geochemical controls. *Petroleum Science and Technology*, 2018, 36(16): 1298-1304.
- Wang, S., Javadpour, F., Feng, Q. Molecular dynamics simulations of oil transport through inorganic nanopores in shale. *Fuel*, 2016, 171: 74-86.
- Wu, H., Chen, J., Liu, H. Molecular dynamics simulations about adsorption and displacement of methane in carbon nanochannels. *The Journal of Physical Chemistry C*, 2015, 119(24): 13652-13657.
- Xiong, H., Devegowda, D., Huang, L. EOR solvent-oil interaction in clay-hosted pores: Insights from molecular dynamics simulations. *Fuel*, 2019, 249: 233-251.
- Xu, H., Yu, H., Fan, J., et al. Enhanced gas recovery in kerogen pyrolytic pore network: Molecular simulations and theoretical analysis. *Energy & Fuels*, 2021, 35(3): 2253-2267.
- Young, T. An essay on the cohesion of fluids. *Philosophical Transactions of the Royal Society of London*, 1805, 95: 65-87.
- Zhang, W., Feng, Q., Wang, S., et al. Oil diffusion in shale

- nanopores: Insight of molecular dynamics simulation. *Journal of Molecular Liquids*, 2019, 290: 111183.
- Zhang, Y., Guo, W. Molecular insight into the tight oil movability in nano-pore throat systems. *Fuel*, 2021, 293: 120428.
- Zhao, J., Yao, G., Ramiseti, S. B., et al. Molecular dynamics investigation of substrate wettability alteration and oil transport in a calcite nanopore. *Fuel*, 2019, 239: 1149-1161.
- Zhong, J., Wang, P., Zhang, Y., et al. Adsorption mechanism of oil components on water-wet mineral surface: A molecular dynamics simulation study. *Energy*, 2013, 59: 295-300.
- Zou, C., Yang, Z., Wang, H., et al. Exploring petroleum inside source kitchen: Jurassic unconventional continental giant shale oil & gas field in Sichuan basin. *Acta Geologica Sinica*, 2019, 93(7): 1551-1562. (in Chinese)